

Holograms for acoustics

[Kai Melde](#), [Andrew G. Mark](#), [Tian Qiu](#) & [Peer Fischer](#) 

[Nature](#) **537**, 518–522 (2016)

39k Accesses | **564** Citations | **412** Altmetric | [Metrics](#)

Abstract

Holographic techniques are fundamental to applications such as volumetric displays¹, high-density data storage and optical tweezers that require spatial control of intricate optical² or acoustic fields^{3,4} within a three-dimensional volume. The basis of holography is spatial storage of the phase and/or amplitude profile of the desired wavefront^{5,6} in a manner that allows that wavefront to be reconstructed by interference when the hologram is illuminated with a suitable coherent source. Modern computer-generated holography⁷ skips the process of recording a hologram from a physical scene, and instead calculates the required phase profile before rendering it for reconstruction. In ultrasound applications, the phase profile is typically generated by discrete and independently driven ultrasound sources^{3,4,8,9,10,11,12}; however, these can only be used in small numbers, which limits the complexity or degrees of freedom that can be attained in the wavefront. Here we introduce monolithic acoustic holograms, which can reconstruct diffraction-limited acoustic pressure fields and thus arbitrary ultrasound beams. We use rapid fabrication to craft the holograms and achieve reconstruction degrees of freedom two orders of magnitude higher than commercial phased array sources. The technique is inexpensive, appropriate for both transmission and reflection elements, and scales well to higher information content, larger aperture size and higher power. The complex three-dimensional pressure and phase distributions produced by

these acoustic holograms allow us to demonstrate new approaches to controlled ultrasonic manipulation of solids in water, and of liquids and solids in air. We expect that acoustic holograms will enable new capabilities in beam-steering and the contactless transfer of power, improve medical imaging, and drive new applications of ultrasound.

This is a preview of subscription content, [access via your institution](#)

Access options

Buy this article

- Purchase on Springer Link
- Instant access to full article PDF

Buy now

Subscribe to this journal

Receive 51 print issues and online access

\$199.00 per year

only \$3.90 per issue

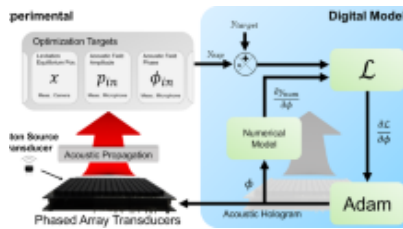
Learn more

Prices may be subject to local taxes which are calculated during checkout

Additional access options:

- [Log in](#)
- [Learn about institutional subscriptions](#)
- [Read our FAQs](#)
- [Contact customer support](#)

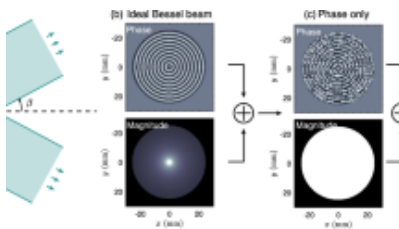
Similar content being viewed by others



A digital twin approach for experimental acoustic hologram optimization

Article | Open access

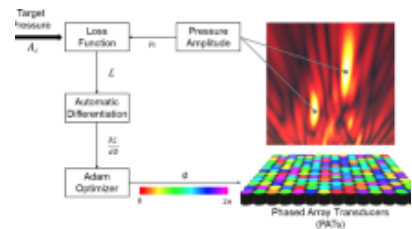
11 January 2024



Generating Bessel beams with broad depth-of-field by using phase-only acoustic holograms

Article | Open access

27 December 2019



Acoustic hologram optimisation using automatic differentiation

Article | Open access

16 June 2021

References

- 1 Tay, S. et al. An updatable holographic three-dimensional display. *Nature* **451**, 694–698 (2008)
- 2 Grier, D. G. A revolution in optical manipulation. *Nature* **424**, 810–816 (2003)
- 3 Marzo, A. et al. Holographic acoustic elements for manipulation of levitated objects. *Nat. Commun.* **6**, 8661 (2015)
- 4 Hertzberg, Y. & Navon, G. Bypassing absorbing objects in focused ultrasound using computer generated holographic technique. *Med. Phys.* **38**, 6407–6415 (2011)
- 5 Gabor, D. A new microscopic principle. *Nature* **161**, 777–778 (1948)

- 6 Leith, E. N. & Upatnieks, J. Reconstructed wavefronts and communication theory. *J. Opt. Soc. Am.* **52**, 1123–1130 (1962)

- 7 Dallas, W. J. in *Digital Holography and Three-Dimensional Display* Ch. 1 (ed. Poon, T.) 1–49 (Springer, 2006)

- 8 Szabo, T. L. *Diagnostic Ultrasound Imaging: Inside Out* 2nd edn (Academic, 2014)

- 9 Drinkwater, B. W. & Wilcox, P. D. Ultrasonic arrays for non-destructive evaluation: a review. *NDT Int.* **39**, 525–541 (2006)

- 10 Demore, C. E. et al. Mechanical evidence of the orbital angular momentum to energy ratio of vortex beams. *Phys. Rev. Lett.* **108**, 194301 (2012)

- 11 Baresch, D., Thomas, J. L. & Marchiano, R. Observation of a single-beam gradient force acoustical trap for elastic particles: acoustical tweezers. *Phys. Rev. Lett.* **116**, 024301 (2016)

- 12 Anhäuser, A., Wunenburger, R. & Brasselet, E. Acoustic rotational manipulation using orbital angular momentum transfer. *Phys. Rev. Lett.* **109**, 034301 (2012)

- 13 Goodman, J. W. *Introduction to Fourier Optics* 3rd edn (Roberts & Co., 2005)

- 14 Xu, L., Peng, X., Guo, Z., Miao, J. & Asundi, A. Imaging analysis of digital holography. *Opt. Express* **13**, 2444–2452 (2005)

- 15 Lesem, L. B., Hirsch, P. M. & Jordan, J. A. The kinoform: a new wavefront reconstruction device. *IBM J. Res. Dev.* **13**, 150–155 (1969)
-
- 16 Mellin, S. & Nordin, G. Limits of scalar diffraction theory and an iterative angular spectrum algorithm for finite aperture diffractive optical element design. *Opt. Express* **8**, 705–722 (2001)
-
- 17 Haist, T., Schonleber, M. & Tiziani, H. J. Computer-generated holograms from 3D-objects written on twisted-nematic liquid crystal displays. *Opt. Commun.* **140**, 299–308 (1997)
-
- 18 Caleap, M. & Drinkwater, B. W. Acoustically trapped colloidal crystals that are reconfigurable in real time. *Proc. Natl Acad. Sci. USA* **111**, 6226–6230 (2014)
-
- 19 Courtney, C. R. P. et al. Manipulation of particles in two dimensions using phase controllable ultrasonic standing waves. *Proc. R. Soc. A*
<http://dx.doi.org/10.1098/rspa.2011.0269> (2011)
-
- 20 Foresti, D., Nabavi, M., Klingauf, M., Ferrari, A. & Poulidakos, D. Acoustophoretic contactless transport and handling of matter in air. *Proc. Natl Acad. Sci. USA* **110**, 12549–12554 (2013)
-
- 21 Oberti, S., Neild, A. & Dual, J. Manipulation of micrometer sized particles within a micromachined fluidic device to form 2D patterns using ultrasound. *J. Acoust. Soc. Am.* **121**, 778–785 (2007)
-

- 22 Lee, J. et al. Single beam acoustic trapping. *Appl. Phys. Lett.* **95**, 073701 (2009)
-
- 23 Courtney, C. R. P. et al. Independent trapping and manipulation of microparticles using dexterous acoustic tweezers. *Appl. Phys. Lett.* **104**, 154103 (2014)
-
- 24 Johnson, L. M. et al. Elastomeric microparticles for acoustic mediated bioseparations. *J. Nanobiotechnol.* **11**, 22 (2013)
-
- 25 Sapozhnikov, O. A. & Bailey, M. R. Radiation force of an arbitrary acoustic beam on an elastic sphere in a fluid. *J. Acoust. Soc. Am.* **133**, 661–676 (2013)
-
- 26 Roichman, Y., Sun, B., Roichman, Y., Amato-Grill, J. & Grier, D. G. Optical forces arising from phase gradients. *Phys. Rev. Lett.* **100**, 013602 (2008)
-
- 27 Chen, X. & Apfel, R. E. Radiation force on a spherical object in an axisymmetric wave field and its application to the calibration of high-frequency transducers. *J. Acoust. Soc. Am.* **99**, 713–724 (1996)
-
- 28 Xie, W. J. & Wei, B. Parametric study of single-axis acoustic levitation. *Appl. Phys. Lett.* **79**, 881–883 (2001)
-
- 29 Tumbleston, J. R. et al. Continuous liquid interface production of 3D objects. *Science* **347**, 1349–1352 (2015)
-

- 30 Studart, A. R. Additive manufacturing of biologically-inspired materials. *Chem. Soc. Rev.* **45**, 359–376 (2016)
-
- 31 Liu, D. L. & Waag, R. C. Propagation and backpropagation for ultrasonic wavefront design. *IEEE Trans. Ultrason. Ferroelectr. Freq. Control* **44**, 1–13 (1997)
-
- 32 Matsushima, K. & Shimobaba, T. Band-limited angular spectrum method for numerical simulation of free-space propagation in far and near fields. *Opt. Express* **17**, 19662–19673 (2009)
-
- 33 Sinha, M. & Buckley, D. J. in *Physical Properties of Polymers Handbook* Ch. 60 (ed. Mark, J. E.) 1021–1031 (Springer, 2007)
-

Acknowledgements

We thank P. Weber and M. Fratz for suggestions. This work was in part supported by the Max Planck Society and by the European Research Council (ERC grant agreement 278213).

Author information

Authors and Affiliations

Max Planck Institute for Intelligent Systems, Heisenbergstrasse 3, Stuttgart, 70569, Germany

Kai Melde, Andrew G. Mark, Tian Qiu & Peer Fischer

Institute for Physical Chemistry, University of Stuttgart, Pfaffenwaldring 55, Stuttgart, 70569, Germany

Peer Fischer

Contributions

P.F. initiated the project. K.M. conceived of the hologram and developed the workflow for the hologram generation. T.Q. fabricated the holograms. K.M. and A.G.M. designed

and performed the experimental demonstrations. P.F. directed the research project. A.G.M., K.M. and P.F. wrote the manuscript.

Corresponding author

Correspondence to [Peer Fischer](#).

Ethics declarations

Competing interests

The authors filed two patent applications related to the use of acoustic holograms.

Additional information

All photographs were taken by the authors. The target image of the dove in [Fig. 1a](#) is a modified rendition of a picture for which the authors hold a commercial license, and is available at <https://www.vectoropenstock.com/vectors/preview/71432/whitedove-laurel-peace-symbol>.

Reviewer Information

Nature thanks B. Drinkwater, A. Nield and the other anonymous reviewer(s) for their contribution to the peer review of this work.

Extended data figures and tables

[**Extended Data Figure 1 Analysis of the 3D print quality.**](#)

a, Map of design thickness ΔT_D from hologram calculation, as sent to the printer. **b**, Measured thickness ΔT_M map from X-ray computed tomography of the printed hologram. Red circles mark sections of inhomogeneous material density. **c**, Difference between design (**a**) and measured (**b**) thicknesses. **d–f**, Comparison of thickness profiles

ΔT for design (blue) and measurement (red) along $y = 10$ mm (**d**), $y = 0$ mm (**e**), and $y = -10$ mm (**f**). The λ scale bar in **d** shows the wavelength in water at 2.06 MHz.

Extended Data Figure 2 Reconstruction of the target image.

a, Virtual reconstruction of the pressure field from the final hologram after IASA. **b**, Hydrophone measurement of the acoustic pressure p , normalized by the highest measured pressure p_{\max} , in the plane $z = 30$ mm.

Extended Data Figure 3 One acoustic hologram can store multiple images in different image planes.

Reconstruction yields all images concurrently. **a**, The calculated synthetic phase map recorded in the hologram. **b–d**, Thermochromic detector measurement of local acoustic intensity of the reconstruction at the three independent image planes. Scale bar, 10 mm (applies to all images). See Methods for more details of the measurement, and [Extended Data Fig. 4](#) for complementary hydrophone scans.

Extended Data Figure 4 Multiple images from one hologram.

a, Hydrophone measurements for each image plane. **b**, Virtual reconstruction of the final hologram.

Extended Data Figure 5 Pictures of levitated objects in air.

a, Aluminium. **b**, Silicon. **c**, Lithium. **d**, Expanded polystyrene. **e, f**, Hollow glass microspheres. **g**, Water mist, aerosolized at the transducer face, **h**, coalesces into droplets trapped in the acoustic field. **i**, Calculated Gor'kov potential, '+' signs indicate points with trapped droplets in **h**. All scale bars, 5 mm. Gravity is acting downwards in all configurations.

Extended Data Figure 6 Radiation forces on spherical silicone particles.

a, Radiation force on a spherical PDMS particle as a function of its radius exposed to a plane travelling wave with frequency $f = 2$ MHz, and amplitude $p_0 = 100$ kPa. **b**, Low-drive-voltage hydrophone measurement of pressure distribution scaled by factor of 2.5 to match conditions used in the trapping experiments. **c**, Detail of section A with force

vectors. **d**, Photograph of particles assembled at the pressure maxima in section A. Scale bar, 1 mm. **e**, Forces in x and z direction along the cut line shown in **c** for different particle radii (see key at top right). **f**, Microscopy image of the PDMS particle suspension used in trapping experiments. Scale bar, 300 μm .

Extended Data Figure 7 Example sections showing force vectors and corresponding photographs of the particle trap in operation.

Panels **a** and **b** show results from sections B and C respectively in [Extended Data Fig. 6b](#). Scale bars, 1 mm.

Extended Data Figure 8 Schematic of the hologram calculation.

a, The transducer output amplitude profile is used as the input boundary condition at the hologram plane. **b, c**, After transmission through the hologram the wavefront is propagated (red lines) to **d, e**, the desired image plane, where it is compared with **f**, the target image, in this case a pure amplitude image of the target image. During hologram optimization the target image amplitude is imposed upon the image plane (the phase is preserved) and then propagated back to the hologram. Again, the amplitude at the hologram plane is set to match that produced by the transducer (accounting for transmission losses) and the process is repeated. After several iterations the optimized reconstructed image (shown here) converges to the target.

Extended Data Figure 9 Experimental set-up for waterborne ultrasound studies.

Experiments were conducted in an open-topped, water-filled glass tank lined on three sides by acoustic absorber. **a**, Side view and **b**, perspective view of the set-up for particle assembly into a target image used to acquire [Fig. 2a](#). The PDMS microparticles are contained within the particle cell located above the hologram. The hologram is mounted on the transducer, which is enclosed in a waterproof box, and projects the soundfield upwards. The cell is arranged so that its upper window coincides with the image plane of the hologram. Photographs and movies are acquired by the camera mounted above the water's surface. **c**, Side view and **d**, perspective view of the set-up

used to demonstrate phase-gradient surfers and acquire [Fig. 3](#). The hologram, mounted on the transducer, projects a soundfield upwards towards the surface of the water. The hologram is positioned so that its image plane is at the water–air interface. Particles travel along the resulting crests, propelled by the projected phase gradient. The motion is captured by the camera located above the surface of the water. Sizes not to scale.

Supplementary information

Acoustic particle assembly

The container, filled with a suspension of silicone particles in water, is positioned above the acoustic hologram with the transducer located in the back. The scene is observed from the top. Initially the sound field is off and the particles are at rest. When the transducer is turned on, the particles collect at the top window of the container (towards observer) and assemble in the form of the “Dove of Peace”. The trapping sites are defined by the projected sound pressure image. When the system is turned off the ensemble collapses and particles settle to the bottom of the container. (MP4 4012 kb)

Acoustic surfers

Two objects, in the form of spherical caps, move along circular paths of opposite direction. The scene is first observed from the side then from above. The outer object has a diameter of 4 mm and the inner object a diameter of 2 mm, with both heights being equal to 0.5 mm. The radii for the inner and outer trajectory are 8 mm and 16 mm, respectively, and the projected acoustic phase gradient for both paths is about 1 rad/mm. This corresponds to a topological charge of +8 for the inner path and -16 for the outer path. The objects will follow the closed contour indefinitely until the transducer is turned off. The same projected phase gradient is then used to propel different objects. The last part demonstrates the effect of an open contour. Observed from above, a blue spherical cap of 4 mm diameter and 0.5 mm height is manually placed at the start of the open trajectory with a phase gradient of about 1 rad/mm. The yellow line marks the tracked particle position in each frame. At the end of the contour the particle is ejected and free to float over the water surface. (MP4 5427 kb)

Wave propagation z-scan

This video shows the amplitude (left) and phase (right) plot of the calculated, propagating acoustic field for the open contour phase gradient image. The video shows the field while scanning along the z-direction. The z coordinate is displayed above the amplitude plot. The image plane is located at $z = 30$ mm. (MP4 11046 kb)

[Double droplet levitation](#)

Close up view of the air cavity with the hologram positioned at the top and the transducer at the bottom. Two water droplets are manually loaded into the traps using a syringe needle. Their diameters are approximately 1.1 mm. (MP4 5553 kb)

PowerPoint slides

[PowerPoint slide for Fig. 1](#)

[PowerPoint slide for Fig. 2](#)

[PowerPoint slide for Fig. 3](#)

[PowerPoint slide for Fig. 4](#)

Rights and permissions

[Reprints and permissions](#)

About this article

Cite this article

Melde, K., Mark, A., Qiu, T. *et al.* Holograms for acoustics. *Nature* **537**, 518–522 (2016).

<https://doi.org/10.1038/nature19755>

Received

23 March 2016

Accepted

12 August 2016

Published

21 September 2016

Issue Date

22 September 2016

DOI

<https://doi.org/10.1038/nature19755>

Subjects

[Acoustics](#)

• [Mechanical engineering](#)

• [Techniques and instrumentation](#)

This article is cited by

[A digital twin approach for experimental acoustic hologram optimization](#)

Tatsuki Fushimi, Daichi Tagami ... Yoichi Ochiai

Communications Engineering (2024)

[Acoustic-driven magnetic skyrmion motion](#)

Yang Yang, Le Zhao ... Tianxiang Nan

Nature Communications (2024)

[Refined acoustic holography via nonlocal metasurfaces](#)

Shuhuan Xie, Hongyu Ma ... Tong Hao

Science China Physics, Mechanics & Astronomy (2024)

[Acoustic microbubble propulsion, train-like assembly and cargo transport](#)

Jakub Janiak, Yuyang Li ... Daniel Ahmed

Nature Communications (2023)

[Phase holograms for the three-dimensional patterning of unconstrained microparticles](#)

Mohamed A. Ghanem, Adam D. Maxwell ... Michael R. Bailey

Scientific Reports (2023)

